Carbonyl Complexes of Iron(II), Ruthenium(II), and Osmium(II) 5,10,15,20-Tetraphenylporphyrinates: A Comparative Investigation by X-ray Crystallography, Solid-State NMR Spectroscopy, and Density Functional Theory

Renzo Salzmann, Christopher J. Ziegler, Nathalie Godbout, Michael T. McMahon, Kenneth S. Suslick, and Eric Oldfield*

Contribution from the Department of Chemistry, University of Illinois at Urbana-Champaign, 600 South Mathews Avenue, Urbana, Illinois 61801

Received November 24, 1997

Abstract: We have synthesized and characterized via single-crystal X-ray diffraction methods iron(II), ruthenium(II), and osmium(II) carbonyl derivatives of (1-methylimidazole)(5,10,15,20-tetraphenylporphyrinate) [(5,10,15,20-tetraphenylporphyrinate = TPP)], Fe(TPP)(CO)(1-MeIm)·toluene, Ru(TPP)(CO)(1-MeIm)· chloroform, and Os(TPP)(CO)(1-MeIm)·chloroform, together with the osmium(II) pyridine adduct Os(TPP)- (CO)(py)·2benzene. The crystallographic results permit a detailed structural comparison between all of the six carbonyl metalloporphyrins which can be prepared from TPP, Fe, Ru, Os, and the two axial bases 1-methylimidazole and pyridine. The structures of all three (Fe, Ru, Os) 1-methylimidazole complexes display major saddle distortions, with the extent of the distortions being Fe > Ru ∼ Os. For the pyridine complexes, deviations from planarity of the porphyrin ring are about an order of magnitude smaller than those for the 1-methylimidazole species. The M−C−O bond angles in all complexes are in the range 176.8−179.3°. We also determined the ^{13}C and ^{17}O NMR isotropic chemical shifts, the ^{13}C NMR chemical shift tensor elements, and, for the three 1-MeIm adducts, the ^{17}O nuclear quadrupole coupling constants. We then used density functional theory (DFT) to relate the experimental spectroscopic results to the experimental structures. For the ^{13}C and ^{17}O isotropic shifts, there are excellent correlations between theory and experiment (^{13}C, R^2 value = ∼0.99; ^{17}O, R^2 value = ∼0.99), although the slopes (^{13}C, ∼−0.97; ^{17}O, ∼−1.27) deviate somewhat from the ideal values. For the ^{17}O nuclear quadrupole coupling constant, our results indicate an rms error between theory and experiment of 0.20 MHz, for experimental values ranging from (+)1.0 to (−)0.40 MHz, where the signs are deduced from the calculations. The ability to predict spectroscopic observables in metalloporphyrin systems having relatively well characterized structures by using density functional theory provides additional confidence in the application of these theoretical methods to systems where structures are much less certain, such as heme proteins.

Introduction

Understanding how small ligand molecules, such as NO, CO, O_2, RNC, and RNO, bind to metal sites in metalloproteins has been a topic of considerable interest for some time.[1−8] In principle, single-crystal X-ray crystallographic studies of proteins should enable a determination of the local geometries of metal−ligand interactions, but the relatively limited resolution of protein crystal structures has resulted in some controversies as to the actual geometries involved. The most studied system is the Fe−CO interaction in heme proteins, where geometries

ranging from essentially linear and untilted to highly bent, have been reported.[9−13] The results of several spectroscopic techniques, such as extended X-ray absorption fine structure (EXAFS)[14] and X-ray absorption near edge spectroscopy (XANES),[15] have supported such bent geometries, while more recent interpretations of infrared data, both in solution[16] and in the crystalline solid-state,[17] have supported undistorted geometries. There is thus interest in clarifying such questions by using other spectroscopic techniques, such as nuclear magnetic resonance spectroscopy[18−20] and Mössbauer spectroscopy.[21]

Synthetic metalloporphyrin compounds can play an important role in facilitating our understanding of heme protein structure,

(1) Filehne, W. *Arch. Exp. Pathol. Pharmakol.* **1878**, *9*, 329−379.
(2) Warburg, O.; Kubouritz, T.; Christian, W. *Biochem. Z.* **1931**, *242*, 170−205.
(3) Jung, F. *Naturwissenschaften* **1940**, *28*, 264−265.
(4) Keilin, D.; Hartree, E. F. *Nature* **1943**, *151*, 390.
(5) Pauling, L.; Coryell, C. D. *Proc. Natl. Acad. Sci. U.S.A.* **1936**, *22*, 210−216.
(6) Pauling, L. *Nature* **1964**, *203*, 182−183.
(7) Weiss, J. J. *Nature* **1964**, *203*, 183.
(8) Perutz, M. *Protein Structure. New Approaches to Disease and Therapy*; W. H. Freeman and Co.: New York, 1992.
(9) Steigemann, W.; Weber, E. In *Hemoglobin and Oxygen Binding*, Ho, C., Ed.; Elsevier Biomedical: New York, 1982; pp 19−24.
(10) Norvell, J. C.; Nunes, A. C.; Schoenborn, B. P. *Science* **1975**, *190*, 568−570.

(11) Kuriyan, J.; Wilz, S.; Karplus, M.; Petsko, G. A. *J. Mol. Biol.* **1986**, *192*, 133−154.
(12) Quillin, M. L.; Arduini, R. M.; Olson, J. S.; Phillips, G. N., Jr. *J. Mol. Biol.* **1993**, *234*, 140−155.
(13) Yang, F.; Phillips, G. N., Jr. *J. Mol. Biol.* **1996**, *256*, 762−774.
(14) Ascone, I.; Bianconi, A.; Dartyge, E.; Della Longa, S.; Fontaine, A.; Momentau, M. *Biochim. Biophys. Acta* **1987**, *915*, 168−171.
(15) Bianconi, A.; Congiu-Castellano, A.; Durham, P. J.; Hasnain, S. S.; Phillips, S. *Nature* **1985**, *318*, 685−687.
(16) Lim, M.; Jackson, T. A.; Anfinrud, P. A. *Science* **1995**, *269*, 962−965.
(17) Ivanov, D.; Sage, J. T.; Keim, M.; Powell, J. R.; Asher, S. A.; Champion, P. M. *J. Am. Chem. Soc.* **1994**, *116*, 4139−4140.

Table 1.   Crystallographic Data Summary

	Fe(TPP)(CO)(1-MeIm)	Ru(TPP)(CO)(1-MeIm)	Ru(TPP)(CO)(1-MeIm)[28]	Os(TPP)(CO)(1-MeIm)	Os(TPP)(CO)(py)
formula	$C_{49}H_{34}N_6OFe \cdot$toluene	$C_{49}H_{34}N_6ORu \cdot CHCl_3$	$C_{49}H_{34}N_6ORu \cdot$toluene	$C_{49}H_{34}N_6O$ Os$\cdot CHCl_3$	$C_{49}H_{34}N_6O$ Os$\cdot$2(benzene)
mol wt	870.81	943.26	916.03	1032.39	1066.23
color	red	purple		purple	black
crystal system	triclinic	orthorhombic	triclinic	orthorhombic	monoclinic
a (Å)	9.76770(10)	9.7228(2)	9.7959(15)	9.7179(2)	13.2059(2)
b (Å)	13.28250(10)	17.6641(3)	13.3197(13)	17.6120(4)	19.3726(4)
c (Å)	17.6251(3)	25.58000(10)	17.6180(16)	25.5891(6)	19.86200(10)
α (deg)	74.7500(10)	90	74.881(9)	90	90
β (deg)	88.3660(10)	90	87.973(10)	90	105.9950(10)
γ (deg)	83.7290(10)	90	83.229(10)	90	90
V (Å^3)	2192.95(5)	4393.22(12)	2203.8(5)	4379.6(2)	4884.63
Z	2	4	2	4	4
D_{calc} (g cm^{-3})	1.319	1.426	1.380	1.566	1.450
space group	$P\bar{1}$	$P2_12_12_1$	$P\bar{1}$	$P2_12_12_1$	$P2_1/c$
radiation, wavelength (Å)	Mo Kα, 0.710 73	Mo Kα, 0. 710 73		Mo Kα, 0. 710 73	Mo Kα, 0. 710 73
μ (mm^{-1})	0.392	0.585		3.140	2.659
crystal size (mm)	0.08 × 0.18 × 0.22	0.04 × 0.04 × 0.46		0.06 × 0.09 × 0.42	0.05 × 0.10 × 0.11
temperature (K)	198(2)	198(2)	153(2)	198(2)	198(2)
diffractometer	Siemens SMART/CCD	Siemens SMART/CCD		Siemens SMART/CCD	Siemens SMART/CCD
no. of data points collected	6798	7699	9049	10441	7660
no. of data points with $I > 2\sigma(I)$	5516	5444		8361	5186
abs min/max	0.816/0.990	0.8654/1.000		0.1360/0.2196	0.0068/0.0233
$R1$	0.0430	0.0886	0.0344	0.0601	0.0523
w$R2$	0.0607	0.1444	0.0939	0.0906	0.0964
GOF	1.175	1.181		1.204	1.154

since the structures of the smaller synthetic analogues generally have smaller uncertainties than the protein crystal structures.[22] Well-characterized model systems can then form a database for interpreting the results of spectroscopic studies of the heme proteins using modern quantum chemical techniques. Here, the recent developments and applications of density functional theory,[23−25] together with recent improvements in computer hardware, and the use of parallel processing[26] show real promise for relating the results of spectroscopic measurements—e.g., infrared[24] and NMR[27]—to structure and, in the future, to function.

There is, however, the need for more complete structural and spectroscopic data on CO-, O$_2$-, RNC-, RNO-, and R$_2$S-containing metalloporphyrins to serve as both the structural and spectroscopic database for quantum chemical calculations. In this paper, we describe the synthesis and characterization via single-crystal X-ray diffraction of three *meso*-tetraphenylpor-

phyrin (TPP) systems: carbonyl(1-methylimidazole)(5,10,15,-20-tetraphenylporphyrinato)iron(II), carbonyl(1-methylimidazole)-(5,10,15,20-tetraphenylporphyrinato)osmium(II), and carbonyl (pyridine)(5,10,15,20-tetraphenylporphyrinato)osmium(II). This enables a comparative study of the six CO complexes which can be made from TPP, Fe/Ru/Os, 1-methylimidazole, and pyridine: Fe(TPP)(CO)(1-MeIm), Ru(TPP)(CO)(1-MeIm),[28] Os(TPP)(CO)(1-MeIm), Fe(TPP)(CO)(py),[29] Ru(TPP)(CO)-(py),[30] and Os(TPP)(CO)(py). In addition, we report the structure of a second form of Ru(TPP)(CO)(1-MeIm), containing a single CHCl$_3$ solvate molecule, which crystallizes in a space group different from that of the toluene solvate reported previously[28] and permits an estimate of the effects of crystal-lattice or intermolecular interactions on structure in these systems.

Experimental Section

All compounds were fully characterized by elemental analysis, field desorption mass spectrometry, UV−visible absorption spectroscopy, and solution and solid-state NMR spectroscopy. Elemental analyses were conducted at the University of Illinois School of Chemical Sciences Microanalytical Laboratory. Field desorption mass spectrometry measurements were made using a Finnigan-MAT (Bremen, Germany) Model 731 instrument. Porphyrin UV−visible spectra were measured using a Hitachi Ltd. (Tokyo, Japan) Model 3300 UV−visible double-monochromator spectrophotometer. The single-crystal X-ray measurements were made using a Siemens (Madison, WI) SMART diffractometer. Solid-state NMR spectra were obtained on "home-built" 360 and 500 MHz spectrometers using Oxford magnets (Oxford Instruments, Osney Mead, U.K.), Tecmag (Houston, TX) pulse programmers, and Doty Scientific (Columbia, SC) probes.

Synthetic Aspects. The syntheses of 5,10,15,20-tetraphenylporphyrin (H$_2$TPP) and of (5,10,15,20-tetraphenylporphyrinato)iron(III)

(18) Scheidt, R. W.; Lee, J. Y. *Struct. Bonding (Berlin)* **1987**, *64*, 1−70.

(19) Park, K. D.; Guo, K.; Adebodun, F.; Chiu, M. L.; Sligar, S. G.; Oldfield, E. *Biochemistry* **1991**, *30*, 2333−2347.

(20) Barrie, P. J.; Gerothanassis, I. P.; Momentau, M.; Hawkes, G. E. *J. Magn. Reson., Ser. B* **1995**, *108*, 185−188.

(21) Gerothanassis, I.; Barrie, P. J.; Momentau, M.; Hawkes, G. E. *J. Am. Chem. Soc.* **1994**, *116*, 11944−11949.

(22) (a) Trautwein, A.; Maeda, Y.; Harris, F. E.; Formanek, H. *Theor. Chim. Acta* **1974**, *36*, 67−76. (b) Trautwein, A. In *Structure and Bonding*; Dunitz, J. D., Hemmerich, P., Holm, R. H., Ibers, J. A., Jørgensen, C. K., Neilands, J. B., Reinen, D., Williams, R. J. P., Eds.; Springer-Verlag: New York, 1974; pp 101−167. (c) Case, D. A.; Huynh, B. H.; Karplus, M. *J. Am. Chem. Soc.* **1979**, *101*, 4433−4453.

(23) Malkin, V. G.; Malkina, O. L.; Casida, M. E.; Salahub, D. R. *J. Am. Chem. Soc.* **1994**, *116*, 5898−5908.

(24) Ghosh, A.; Bocian, D. F. *J. Phys. Chem.* **1996**, *100*, 6363−6367.

(25) Rovira, C.; Ballone, P.; Parrinello, M. *Chem. Phys. Lett.* **1997**, *271*, 247−250.

(26) Frisch, M. J.; Trucks, G. W.; Head-Gordon, M.; Gill, P. M. W.; Wong, M. W.; Foresman, J. B.; Johnson, B. G.; Schlegel, H. B.; Robb, M. A.; Repiogle, E. S.; Gomperts, R.; Andres, J. L.; Raghavachari, K.; Binkley, J. S.; Gonzalez, C.; Martin, R. L.; Fox, D. J.; Defrees, D. J.; Baker, J.; Stewart, J. J. P.; Pople, J. A. *Gaussian 94/DFT*; Gaussian, Inc.: Pittsburgh, PA, 1994.

(27) Oldfield, E. *J. Biomol. NMR* **1995**, *5*, 217−225.

(28) Slebodnick, C.; Seok, W. K.; Kim, K.; Ibers, J. A. *Inorg. Chim. Acta* **1996**, *57*, 243.

(29) Ping, S.-M.; Ibers, J. A. *J. Am. Chem. Soc.* **1976**, *98*, 8032−8036.

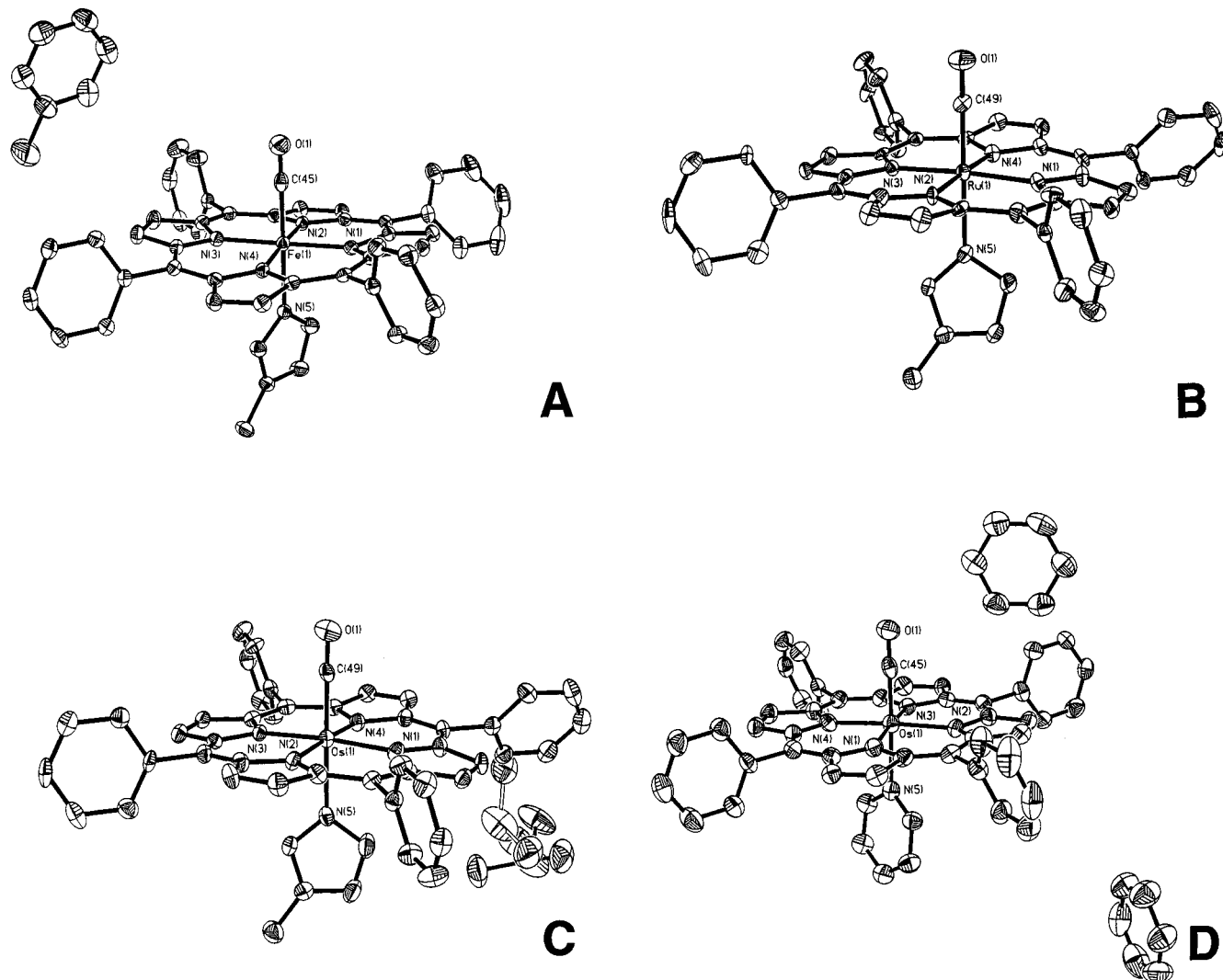(30) Little, R. G.; Ibers, J. A. *J. Am. Chem. Soc.* **1973**, *95*, 8583−8596.

Figure 1. ORTEP structures of (A) carbonyl(1-methylimidazole)(tetraphenylporphyrinato)iron(II)−toluene, (B) carbonyl(1-methylimidazole)-(tetraphenylporphyrinato)ruthenium(II)−chloroform, (C) carbonyl(1-methylimidazole)(tetraphenylporphyrinato)osmium(II)−chloroform (disordered solvent molecule), and (D) carbonyl(pyridine)(tetraphenylporphyrinato)osmium(II)−2(benzene).

chloride [Fe(TPP)(Cl)] were based on modifications of the work of Adler and Dolphin.[31−33]

(a) Carbonyl(1-methylimidazole)(5,10,15,20-tetraphenylporphyrinato)iron(II). Reduced iron porphyrins are extremely sensitive to air and solvent impurities. All solvents used in the reduction of Fe-(TPP)(Cl) were therefore purified by distillation: benzene, over calcium hydride; toluene and heptane, over sodium; and pentane, over sodium benzophenone ketyl. Ethanol was used for the reduction of Fe(TPP)-(Cl) without further purification and was purchased from the McCormick Distillation Co. (Weston, MI). All solvents used in the reductions were freeze/pump/thaw degassed prior to use. Fe(TPP) was generated from Fe(TPP)(Cl) using Cr(acac)$_2$ as the reductant. All syntheses and manipulations of Fe(TPP) and reduced iron porphyrins were conducted in a glovebox or in a Schlenk apparatus under rigorously anaerobic and dry conditions. Cr(acac)$_2$ was synthesized using a literature technique,[34] as modified by Chen.[35]

The Fe(TPP) so produced was then dissolved in toluene, a 2-fold excess of 1-methylimidazole was added, and after three freeze/pump/

thaw cycles, ^{13}CO or C^{17}O gas (Isotec, Miamisburg, OH) was transferred via a gastight syringe into the Schlenk flask. Careful layering of a 5-fold excess of pentane resulted in crystallization of carbonyl (1-methylimidazole)(5,10,15,20-tetraphenylporphyrinato)iron(II) after 4 days at room temperature. Anal. Found (calcd) for Fe(TPP)(CO)-(1-MeIm)·toluene: C, 77.31 (77.24); H, 4.71 (4.86); N, 9.67 (9.65). IR (ν_{CO} in CD$_2$Cl$_2$): 1969 cm^{-1}. ^{13}C NMR (CO): 204.1 ppm.

(b) Carbonyl(1-methylimidazole)(5,10,15,20-tetraphenylporphyrinato)ruthenium(II). The ruthenium porphyrin complex was generated from the ethanol adduct Ru(TPP)(CO)(EtOH)[36] as follows. First, the 1-methylimidazole complex (Ru(TPP)(CO)(1-MeIm)) was isolated from a solution of 50 mg of the ethanol complex in 5% v/v 1-methylimidazole in CHCl$_3$ by addition of heptane. For isotopic labeling, crystals were collected and redissolved in 50 mL of toluene. This toluene solution was then placed in a water-cooled Schlenk flask under 1 atm of either ^{13}CO or C^{17}O and irradiated with a 300 W xenon arc lamp (filtered from IR and UV, 360 nm) for ∼30 min. FTIR measurements indicated complete exchange of the unlabeled CO with ^{13}CO or C^{17}O. The toluene solution was then reduced in volume and the resultant labeled compound crystallized by layering of heptane. Yield: 40 mg of Ru(TPP)(CO)(1-MeIm)·CHCl$_3$ (77%). Anal. Found (calcd) for Ru(TPP)(CO)(1-MeIm)·CHCl$_3$: C, 63.42 (63.66); H, 3.84 (3.74); N, 8.97 (8.91). IR (ν_{CO} in CD$_2$Cl$_2$): 1936 cm^{-1}. ^{13}C NMR (CO): 178.5 ppm.

(31) Abbreviations used: TPP, 5,10,15,20-tetraphenylporphyrinate-(2−); 1-MeIm, 1-methylimidazole; py, pyridine.

(32) (a) Adler, A. D.; Longo, F. R.; Finarelli, J. D.; Goldmacher, J.; Assour, J.; Korsakoff, J. *J. Org. Chem.* **1967**, *32*, 476. (b) Adler, A. D.; Longo, F. R.; Kampas, F.; Kim, J. *J. Inorg. Nucl. Chem.* **1970**, *32*, 2443−2445.

(33) Rousseau, K.; Dolphin, D. *Tetrahedron Lett.* **1974**, *48*, 4251−4254.

(34) Ocone, L. R.; Block, B. P. *Inorg. Synth.* **1966**, *8*, 125−130.

(35) Chen, C. T. Ph.D. Thesis, University of Illinois at Urbana-Champaign, 1992.

(36) Barley, M.; Becker, J. Y.; Domazetis, G.; Dolphin, D.; James, B. R. *Can. J. Chem.* **1983**, *61*, 2389−2396.

Table 2. Structural Summary for Fe, Ru, and Os Porphyrins[a]

	M(TPP)(CO)(1-MeIm)				M(TPP)(CO)(py)		
	M = Fe	M = Ru	M = Ru[28]	M = Os	M = Fe[29]	M = Ru[30]	M = Os
M−N(1)	2.009(2)	2.063(7)	2.053(2)	2.054(6)	2.05(1)	2.057(6)	2.068(6)
M−N(2)	1.999(2)	2.065(6)	2.060(2)	2.047(6)	1.99(1)	2.055(6)	2.0676)
M−N(3)	2.006(2)	2.051(7)	2.052(2)	2.060(6)	2.00(1)	2.058(5)	2.054(6)
M−N(4)	1.999(2)	2.055(7)	2.066(2)	2.047(6)	2.02(1)	2.038(6)	2.060(6)
M−N(5)	2.071(2)	2.185(8)	2.187(2)	2.175(7)	2.10(1)	2.193(4)	2.194(6)
M−C	1.793(3)	1.830(10)	1.828(2)	1.846(6)	1.77(2)	1.838(9)	1.817(9)
C−O	1.061(3)	1.142(10)	1.147(3)	1.150(10)	1.12(2)	1.141(10)	1.190(9)
C−O, riding model[52]	1.095	1.181		1.186			1.225
N(1)-M−N(2)	89.6(2)	90.0(3)	89.40(7)	90.3(3)	89.1(5)	89.8(2)	90.0(3)
N(1)-M−N(3)	179.2(2)	175.8(3)	175.26(7)	174.9(3)	179.4(6)	177.2(2)	175.2(3)
N(1)-M−N(4)	90.3(2)	89.8(3)	90.34(7)	89.5(3)	90.0(5)	89.8(2)	90.3(3)
N(2)-M−N(3)	90.6(2)	90.0(3)	90.84(7)	89.8(3)	91.3(5)	89.8(2)	89.7(3)
N(2)-M−N(4)	176.1(2)	177.9(3)	178.88(7)	176.9(3)	178.3(6)	175.2(2)	176.6(3)
N(3)-M−N(4)	89.4(2)	90.4(3)	89.33(7)	90.1(3)	89.7(5)	90.3(2)	89.7(3)
C−M-N(1)	89.8(2)	91.7(4)	92.18(9)	92.4(4)	90.0(8)	92.3(3)	91.8(3)
C−M-N(2)	91.9(2)	90.0(3)	90.42(9)	91.3(3)	89.4(7)	90.5(3)	91.2(3)
C−M-N(3)	89.5(2)	92.5(4)	92.55(9)	92.6(4)	90.5(9)	92.7(3)	93.0(4)
C−M-N(4)	92.0(2)	92.0(3)	90.68(9)	91.7(5)	92.0(7)	92.1(3)	92.2(4)
C−M-N(5)	178.3(2)	176.7(4)	177.83(8)	177.5(4)	177.5(8)	178.9(3)	177.6(4)
M−C−O	179.3(3)	178.6(8)	179.3(2)	176.8(9)	179(2)	178.4(7)	178.3(7)
torsion amplitudes of TPP phenyl rings	1, 8, 10, 26	10, 12, 16, 30	10, 12, 16, 30	8, 12, 15, 28	3, 6, 9, 14	1, 2, 3, 8	4, 7, 14, 16
angle between imidazole ring and porphyrin plane	83	80	80	81	80	88	80

[a] Distances are given in angstroms; angles and torsion amplitudes are given in degrees.

(c) Carbonyl(1-methylimidazole)(5,10,15,20-tetraphenylporphyrinato)osmium(II). The osmium precursor was also generated using a modified literature procedure,[37] from H₂TPP and osmium carbonyl. Carbonyl(1-methylimidazole)(5,10,15,20-tetraphenylporphyrinato)osmium(II) and labeled samples were synthesized in the same manner as the Ru analogues. Suitable crystals were obtained from slow diffusion of pentane into a chloroform solution over 3 days. Anal. Found (calcd) for Os(TPP)(CO)(1-MeIm)·CHCl₃: C, 58.09 (58.45); H, 3.29 (3.42); N, 8.14 (8.01). IR (ν_{CO} in CD₂Cl₂): 1899 cm⁻¹. ¹³C NMR (CO): 142.6 ppm.

(d) Carbonyl(pyridine)(5,10,15,20-tetraphenylporphyrinato)osmium(II). This compound was synthesized in the same manner as Os(TPP)(CO)(1-MeIm), but employing pyridine as the axial base. Suitable crystals were obtained from slow diffusion of pentane into a benzene solution over 5 days. Anal. Found (calcd) for Os(TPP)(CO)-(py)·2(benzene): C, 69.79 (69.89); H, 4.13 (4.26); N, 6.47 (6.69). IR (ν_{CO} in CD₂Cl₂): 1912 cm⁻¹. ¹³C NMR (CO): 142.9 ppm.

Crystallographic Aspects. Single-crystal data for the four systems described above were collected on a Siemens (Madison, WI) SMART/CCD diffractometer using MoKα radiation (λ = 0.710 73 Å). The structures were solved using the SHELXTL V5.0 (Siemens) system and refined by full-matrix least-squares procedures on F^2 using all reflections. The data were corrected for Lorentz and polarization effects, and an empirical absorption correction was applied.

The color and morphology of the crystals, the crystallographic systems and space groups, and other information related to the crystal structure determinations are summarized in Table 1. In general, from 6798 to 10 441 data points were collected using the area detector, and from 5186 to 8361 data points having $I > 2\sigma(I)$ were used in the refinements. The final R1 values varied from 0.0430 to 0.0886 and the GOF values from 1.154 to 1.204, Table 1. (See Supporting Information.) Atomic coordinates, bond lengths angles, and thermal parameters have also been deposited with the Cambridge Crystallographic Data Centre (CCDC). Any request to the CCDC for this material should quote the full literature citation and the reference number.

Computations. The shielding tensor and electric field gradient (efg) calculations were performed using density functional theory as implemented in the Gaussian 94 program.[26] The NMR shielding tensors were calculated using the gauge-including atomic orbital (GIAO)

method,[38] using Becke's exchange functional[39] and Perdew and Wang's gradient-corrected correlation functional[40] ("BPW91" exchange and correlation functional). For both the shifts and the efg, we used a locally dense approach[41] in which the metal was represented by an effective core potential (ECP), or an all-electron basis set, and two or three sets of functions were employed for the other atoms.

In initial calculations, we carried out a constrained geometry optimization of the Fe(TPP)(CO)(1-MeIm) model, in which only the Fe−C and C−O bond lengths were allowed to change, by using Becke's three-parameter functional[42] with the Lee, Parr, and Yang correlation functional[43] ("B3LYP" exchange and correlation functional). For this calculation, we used Wachters' (62111111/331211/3111/3) iron basis set,[44,45] which we modified to (62111111/3311111/3111) by decontracting the p-type functions (to add flexibility) and removing the f-type functions. The Wachters' cobalt basis set was similarly modified and used successfully in our previous study of cobalt-59 shielding.[46] Other basis sets were 6-31G* on the CO ligand and the nitrogen atoms coordinated to iron and 3-21G on the remaining atoms (including the phenyl groups). The shielding tensor calculations for the Fe(TPP)-(CO)(1-MeIm) models were carried out by including phenyl groups on the porphyrin ring and using the following basis set scheme: Wachters' iron basis set, 6-311++G(2d) on the CO ligand and the nitrogen atoms coordinated to iron, 6-31G* on the carbons bonded to

(37) Che, C. M.; Poon, C. K.; Chung, W. C.; Gray, H. B. *Inorg. Chem.* **1985**, *24*, 1277−1278.

(38) Cheesman, J. R.; Trucks, G. W.; Keith, T. A.; Frisch, J. *J. Chem. Phys.* **1996**, *104*, 5497−5509.

(39) Becke, A. D. *Phys. Rev. A* **1988**, *38*, 3098−3100.

(40) Perdew, J. P.; Wang, Y. *Phys. Rev. B* **1992**, *45*, 13244−13249.

(41) Chesnut, D. B.; Moore, K. D. *J. Comput. Chem.* **1989**, *10*, 648−659.

(42) Becke, A. D. *J. Chem. Phys.* **1993**, *98*, 5648−5652.

(43) (a) Lee, C.; Yang, W.; Parr, R. G. *Phys. Rev. B* **1988**, *37*, 785−789. (b) Miehlich, B.; Savin, A.; Stoll, H.; Preuss, H. *Chem. Phys. Lett.* **1989**, *157*, 200−206.

(44) Wachters, A. J. H. *J. Chem. Phys.* **1970**, *52*, 1033−1036; *IBM Tech. Rept. RJ584* **1969**.

(45) Basis sets were obtained from the Extensible Computational Chemistry Environment Basis Set Database, Version 1.0, as developed and distributed by the Molecular Science Computing Facility, Environmental and Molecular Sciences Laboratory, which is part of the Pacific Northwest Laboratory, P.O. Box 999, Richland, WA 99352, and is funded by the U.S. Department of Energy. The Pacific Northwest Laboratory is a multiprogram laboratory operated by Battelle Memorial Institute for the U.S. Department of Energy under Contract DE-AC06-76RLO 1830. Contact David Feller, Karen Schuchardt, or Don Jones for further information.

(46) Godbout, N.; Oldfield, E. *J. Am. Chem. Soc.* **1997**, *119*, 8065−8069.
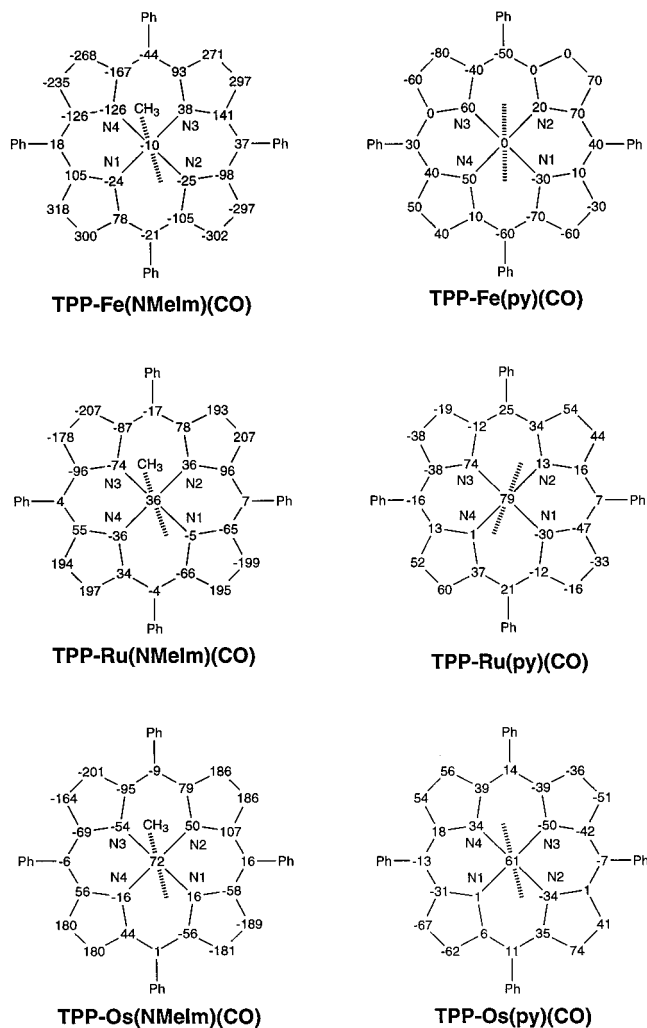
Figure 2. Structures showing deviations from planarity of all of the six carbonyl metalloporphyrins which can be prepared from tetraphenylporphyrin, iron, ruthenium, osmium, 1-methylimidazole, pyridine, and carbon monoxide. The numbers shown are the deviations (in mÅ) from the least-squares porphyrin plane, and the positive numbers indicate a displacement toward the CO ligand. The uncertainties vary from ~2 to 10 mÅ (Table 2).

the nitrogens, and 3-21G* on the remaining atoms (for a total of 797 basis functions). We then investigated shielding using a slightly modified porphyrin, Fe(C$_2$Cap)(CO)(1-MeIm), in which the phenyl groups of the porphyrin ring were replaced by hydrogens, using Wachters' iron basis set, 6-311++G(2d) on the CO ligand, and 6-31G* on the remaining atoms. These initial calculations gave useful information on the sensitivity of the calculations to small structural differences.

Several effective core potentials (ECPs) for the metals were also considered. For iron, we used the Los Alamos (LANL2) ECP with the double-ζ (DZ) basis set,[26,47] with a (42111/2111/311) basis set decontracted from (441/311/41), while the Stuttgart ECP[48] used a (311111/22111/411) basis set. A variety of other basis set test schemes were used on the main elements, and details are given under Results and Discussion.

We then evaluated all of the Fe, Ru, and Os shielding and efg results using a unified approach, based on these exploratory studies. Specifically, we generated two sets of constrained geometry-optimized structures (LANL2DZ ECPs on the metal and a locally dense scheme for the light atoms) using either the BPW91 or B3LYP functional, followed by property evaluations using the BPW91 functional, which

(47) Hay, P. J.; Wadt, W. R. *J. Chem. Phys.* **1985**, *82*, 284−298.
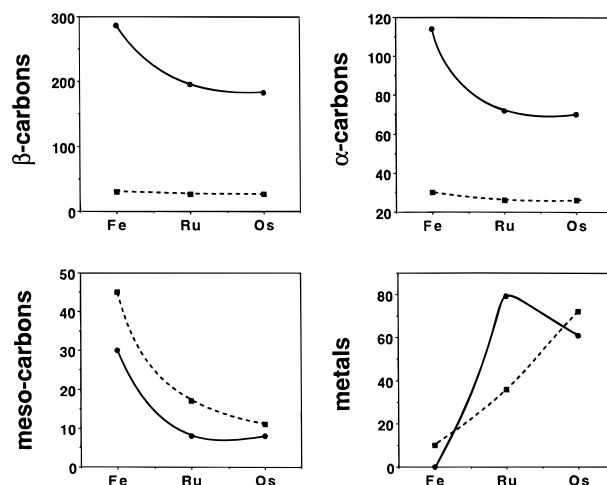(48) Dolg, M.; Wedig, U.; Stoll, H.; Preuss, H. *J. Chem. Phys.* **1987**, *86*, 866−872.

Figure 3. Plots showing the mean absolute deviations from planarity (in mÅ) for iron, ruthenium, and osmium metalloporphyrins containing 1-methylimidazole (solid lines) and pyridine (dashed lines) as axial bases.

in previous work[49] we have found to give best accord between theory and experiment, in metal−olefin complexes.[49] Calculations here were performed using modifications of the crystallographic structures in which the phenyl groups were replaced by hydrogen atoms, an approximation which again is discussed in more detail below. Calculations were performed on a cluster of Silicon Graphics/Cray (Mountain View, CA) Origin-200 workstations in this laboratory and on Silicon Graphics/Cray Origin-2000 and Power Challenge computers at the National Center for Supercomputing Applications, located in Urbana, IL.

Results and Discussion

We have synthesized and structurally characterized three new porphyrin compounds, the Fe and Os complexes of TPP with 1-methylimidazole and CO as axial ligands, together with the Os−CO−pyridine complex, in addition to determining the structure of Ru(TPP)(CO)(1-MeIm)·CHCl$_3$ in the $P2_12_12_1$ space group. The ORTEP structures of these four molecules are shown in Figure 1. The availability of these new structures now permits a comparison of the structures of all six possible pyridine and 1-methylimidazole adducts of Fe, Ru, and Os with TPP and CO, and selected metric details are given in Table 2.

The most striking feature which can be seen from these results is that all three 1-methylimidazole adducts have significant saddle distortions, while all three pyridine adducts have much smaller distortions. The deviations of each of the porphyrin heavy atoms, as well as the central metal atoms, from the least-squares plane of each macrocycle are shown in Figure 2.

The largest distortions seen are in the Fe(TPP)(CO)(1-MeIm) complex, where the C$^\beta$ atoms are on average ~0.286 Å from the mean plane, to be compared with only ~0.049 Å in the case of Fe(TPP)(CO)(py),[29] Figure 2. In the Ru complexes, the mean deviations are 0.196 Å (1-MeIm) versus 0.04 Å (py), and in the Os complexes, 0.183 Å (1-MeIm) versus 0.055 Å, Figure 2. This is shown graphically in Figure 3, together with additional results for C$^\alpha$, the *meso*-carbons, as well as the metal centers themselves.

The observation that the smallest, iron-containing metallocycle has the largest saddle distortion is not unreasonable, given current ideas about the forces that influence porphyrin planarity. The high charge density on the smaller Fe(II) results in shorter metal (M)−N(porphyrin), M−N(ligand), and M−C bond lengths,

(49) Havlin, R.; McMahon, M.; Srinivasan, R.; Le, H.; Oldfield, E. *J. Phys. Chem. A* **1997**, *101*, 8908−8913.
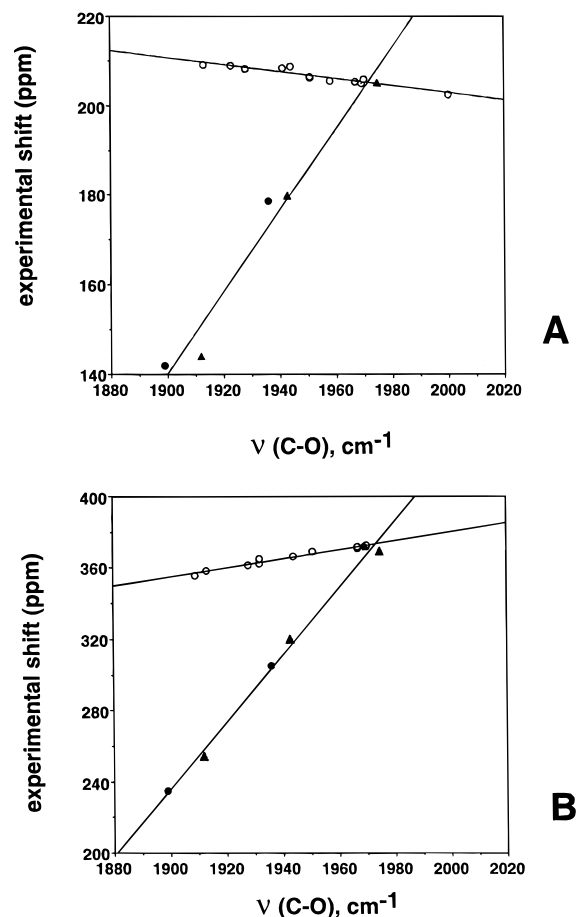
Table 3. Experimental ^{13}C and ^{17}O Shift Parameters and Infrared Vibrational Stretch Frequencies for Model Porphyrins

	^{13}C shifts (ppm)					^{17}O δ_i	IR ν_{CO}
system	δ_i	δ_{11}	δ_{22}	δ_{33}	$|\delta_{33} - \delta_{11}|$	(ppm)	(cm^{-1})
Fe(TPP)(CO)(1-MeIm)	205	370	342	−98	468	372	1969
Fe(TPP)(CO)(py)	205	386	328	−100	486	369	1975
Ru(TPP)(CO)(1-MeIm)	178.7	334	334	−132	466	305	1936
Ru(TPP)(CO)(py)	179.7	338	338	−136	474	320	1943
Os(TPP)(CO)(1-MeIm)	142.2	299	299	−171	470	235	1899
Os(TPP)(CO)(py)	144	300	300	−168	468	254	1912
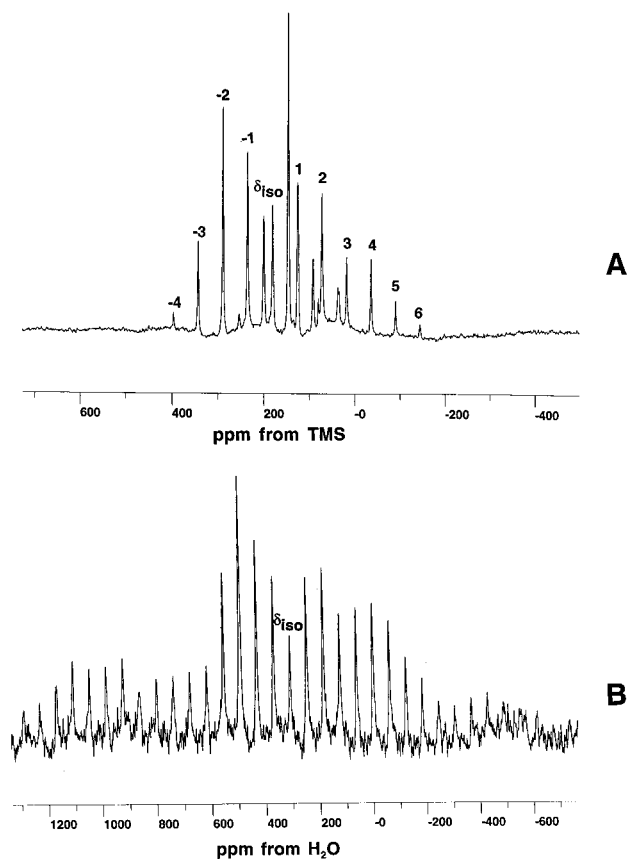
Figure 4. Carbon-13 and oxygen-17 magic angle sample-spinning NMR spectra of ^{13}C- and ^{17}O-labeled metalloporphyrins: (A) ^{13}C MAS NMR spectrum of carbonyl(1-methylimidazole)(5,10,15,20-tetraphenylporphyrinato)ruthenium(II); (B) ^{17}O MAS NMR spectrum of carbonyl(1-methylimidazole)(5,10,15,20-tetraphenylporphyrinato)-ruthenium(II).

Figure 5. Graphs showing correlations between the infrared vibrational stretch frequencies, ν_{CO}, and the experimental carbon-13 and oxygen-17 NMR chemical shifts, for metalloporphyrins and metalloproteins. (A) correlations for carbon-13 shifts in proteins and metalloporphyrin complexes: ●, pyridine metalloporphyrin complexes; ▲, 1-MeIm metalloporphyrin complexes; ○, heme metalloproteins. (B) As for (A) but for oxygen-17. The metalloprotein data points are from ref 19.

which results in a saddle distortion. This can be clearly seen in the M−N(1−5) and M−C bond lengths reported in Table 2. For example, the average Fe−N$_p$ bond length in Fe(TPP)(CO)-(1-MeIm) is 2.003 Å and the Fe−N$_{Im}$ bond length is 2.071 Å, to be compared with average values for the Ru− and Os−1-MeIm complexes of 2.056 Å and the much longer M−N$_{Im}$ values of 2.182 Å, increases of between ∼0.05 and 0.10 Å. In addition, the Fe−C bond is shorter, 1.793(3) Å versus 1.835 Å, a ∼0.04 Å difference. The increased saddle distortions can thus be rationalized on the basis of a core contraction which enables stronger Fe−C,N bonding.

The picture becomes more complex, however, when the structural results for the 1-MeIm complexes are compared with those obtained for the pyridine adducts, Table 2. Here, there appears to be no major difference in M−N$_p$ bond lengths between the pyridine and 1-methylimidazole adducts. For example, for the Ru and Os systems, we find mean bond lengths of $\bar{d}$(M−N$_p$) = 2.056 Å for the 1-MeIm adducts versus $\bar{d}$(M−N$_p$) = 2.057 Å for the pyridine complexes, Table 2, and

differences between the Fe and the Ru and Os $\bar{d}$(M−N$_p$) of 0.042 Å, essentially the same as the 0.053 Å seen for the 1-MeIm complexes. Thus, on the basis of the $\bar{d}$(M−N$_p$) values, the origins of the major changes in porphyrin distortion between the Ru and Os 1-methylimidazole and pyridine complexes is unclear. Similarly, the d(M−N$_5$) differences between the Ru and Os 1-MeIm/py complexes are only 0.01 Å, and the d(M−C) differences are even less.

These results indicate that a simple model in which the M−N bond lengths dominate the porphyrin distortions is likely to be incomplete, since the Fe, Ru, and Os geometries about the central metal atom are very similar in the 1-methylimidazole and pyridine complexes. Either a more subtle steric or electronic effect from the axial base plays a significant role in influencing the porphyrin distortions, or crystal lattice packing effects are important. Clearly, further work of a theoretical nature is needed

Table 4. Theoretical ^{13}C and [17]O Shifts (ppm) for Model Iron 1-Methylimidazole Porphyrins as a Function of the Structure, Basis Sets, and Effective Core Potentials Used[a]

		[13]C				[17]O			
calculation no.	system	δ_i	δ_{11}	δ_{22}	δ_{33}	δ_i	δ_{11}	δ_{22}	δ_{33}
1	Fe(TPP)[b]	198.0	359.6	356.7	−122.2	333.0	571.7	570.6	−143.2
				Structural Effects					
2	Fe(TPP)[b] (g-opt)	215.2	385.2	382.5	−122.2	378.7	639.1	637.6	−140.5
3	Fe(P)[b]	196.9	359.3	356.0	−124.5	333.0	573.1	571.6	−145.6
4	Fe(P)[b] (X-ray)	186.8	344.4	341.2	−125.2	309.7	538.7	537.8	−147.3
5	Fe(C$_2$Cap)	211.9	382.6	380.1	−126.9	368.1	623.6	622.2	−141.4
				Basis Set Effects					
6	Fe(P)[c]	197.0	359.5	356.2	−124.7	333.0	573.2	571.5	−145.5
7	Fe(P)[d]	167.6	312.1	307.1	−116.3	320.6	548.4	544.5	−131.1
8	Fe(P)[e]	170.2	320.9	309.7	−120.2	313.5	541.8	536.5	−137.7
9	Fe(P)[f]	187.1	344.2	332.6	−115.5	323.1	551.8	547.0	−129.4
10	Fe(P)[g]	198.8	358.0	356.1	−117.6	333.3	564.4	563.6	−128.1
11	Fe(P)[h]	200.2	360.2	359.1	−118.8	332.4	563.6	562.8	−129.1
	exptl	205	370	342	−98	372			

[a] Unless otherwise specified, riding model geometry and BPW91 XC functionals were employed. [b] Fe Wachters/6-311++G(2d) CO and N/6-31G* C (bond to N)/3-21G* others. [c] Fe Wachters/6-311++G(2d) CO and N/6-31G* C (ring)/3-21G* H. [d] Fe Stuttgart ECP with (311111/22111/411) basis set/6-311++G(2d) CO and N/6-31G* C (bond to N)/3-21G* others. [e] Fe LANL2 ECP with (42111/2111/311) basis set/6-311++G(2d) CO and N/6-31G* C (bond to N)/3-21G* others. [f] Fe LANL2 ECP with DZ basis set/6-311++G(2d) CO and N/6-31G* C (bond to N)/3-21G* others. [g] Fe LANL2 ECP with DZ basis set/6-311++G(2d) CO/6-31G*N and C (bond to N)/3-21G* others. [h] Fe LANL2 ECP with DZ basis set/6-311++G(2d) CO/6-31G* N/3-21G* others

Table 5. Selected X-ray and Partial Geometry Optimization[a] Structural Parameters of Model Porphyrins (Å)

	X-ray		BPW91		B3LYP	
system	d(M−C)	d(C−O)	d(M−C)	d(C−O)	d(M−C)	d(C−O)
Fe(P)(CO)(1-MeIm)	1.7929	1.061	1.7428 (1.7411)[b]	1.1670 (1.1686)[b]	1.8013 (1.8053)[c]	1.1472 (1.1495)[c]
Fe(P)(CO)(py)	1.7755	1.1285	1.7444	1.1664	1.8009	1.1470
Ru(P)(CO)(1-MeIm)	1.8311	1.1418	1.8600	1.1708	1.8755	1.1561
Ru(P)(CO)(py)	1.8373	1.1423	1.8628	1.1703	1.8779	1.1555
Os(P)(CO)(1-MeIm)	1.8453	1.1508	1.8689	1.1763	1.8740	1.1632
Os(P)(CO)(py)	1.8185	1.1897	1.8686	1.1754	1.8731	1.1624

[a] The partial geometry optimizations were done using the LANL2DZ ECP for the metals, 6-31G* for the CO ligand and the nitrogens, and 3-21G* on the remaining atoms. [b] This structure was obtained using the LANL2DZ ECP on Fe, 6-31G* on C, N, and O, and 3-21G* on H (and shows the influence of a locally dense scheme on the geometry optimization). [c] This structure was obtained using the Wachters basis set on Fe, 6-31G* on CO and nitrogens, and 3-21G on the other atoms (and shows the effect of the ECP on the geometry optimization).

to quantitate such effects. Rovira et al.[25] recently reported the results of Carr−Parrinello molecular dynamics geometry optimization studies on Fe(porphyrin)(CO)(imidazole), whose experimental structure is unfortunately not yet known, so that it is reasonable to suppose that the structures of even larger systems (whose structures are known) should become tractable in the not-too-distant future. As for the effects of crystal lattice packing, inspection of the 1-MeIm and py structures reveals no dramatic changes in crystal packing, unlike the case with e.g. nickel(II) octaethylporphyrin,[50] where major porphyrin distortions are associated with large changes in lattice packing.

Also of interest in Figures 2 and 3 is the observation that the positions of the C$_{meso}$ are far less distorted from the mean plane for Os vs Ru vs Fe, with the 1-methylimidazole and pyridine values being remarkably similar. At the same time, the metal atoms themselves become located higher above the mean plane (toward CO), as noted previously for Ru by Ibers et al.[51]

We should also note at this point that the structural parameters of the two Ru(TPP)(CO)(1-MeIm) molecules shown in Table 2, obtained by different groups on systems having different solvent molecules (CHCl$_3$, toluene) and crystallizing in different space groups ($P2_12_12_1$, $P\bar{1}$), are nevertheless very similar. On

average, there is a 0.005 Å difference in the key bond lengths shown in Table 2 and a 0.7° difference in the key bond angles. The agreement may be even closer though, since our standard deviations are ~3−4 times higher than those reported for the toluene structure.[28]

In all seven structures, the mean M−C−O bond angle is 178.5° with a standard deviation of 0.8°. The C−O bond lengths do, however, appear to vary. The shortest C−O bond length seen is that in Fe(TPP)(CO)(1-MeIm), while the longest is in Os(CO)(py)(TPP). The 1.061(3) Å value determined for Fe(CO)(1-MeIm)(TPP) is surprisingly short, since most C−O bond lengths in Fe porphyrins are in the range 1.107(13)−1.161-(8) Å.[28] We therefore selected a second crystal and carried out a second independent structure determination, but with the same result. Such apparent shortening of terminal groups may be due to anisotropic thermal motions, and mathematical (so-called "riding") corrections have been used previously by Schomaker and Trueblood[52] and Mason et al.[53] to account in part for such effects. We therefore re-refined all four structures using a riding correction for CO. In this case, the Fe(CO)(1-MeIm)(TPP) C−O bond length increased to 1.095 Å, and this and the other riding model corrected C−O bond lengths are shown in Table 2.

(50) (a) Cullen D. L.; Meyer, E. F., Jr. *J. Am. Chem. Soc.* **1974**, *96*, 2095−2102. (b) Scheidt, R. W.; Mondal, J. U.; Eigenbrot, C. W.; Adler, A.; Radonovich, L. J.; Hoard, J. L. *Inorg. Chem.* **1986**, *25*, 795−799.
(51) Bonnet, J. J.; Eaton, S. S.; Eaton, G. R.; Holm, R. H.; Ibers, J. A. *J. Am. Chem. Soc.* **1973**, *95*, 2141−2149.

(52) Schomaker, V.; Trueblood, K. N. *Acta Crystallogr.* **1968**, *B24*, 63−76.
(53) Groombridge, C. J.; Larkworthy, L. F.; Mason, J. *Inorg. Chem.* **1993**, *32*, 379−380.

Table 6. G94/DFT BPW91[a] Calculated ^{13}C and ^{17}O Shieldings (ppm) for Fe, Ru, and Os Carbonyl Metalloporphyrins Containing 1-Methylimidazole or Pyridine at the X-ray, Riding, and Geometry-Optimized Structures

system		^{13}C shieldings					^{17}O shieldings				
		σ_i	σ_{11}	σ_{22}	σ_{33}	$|\sigma_{33}-\sigma_{11}|$	σ_i	σ_{11}	σ_{22}	σ_{33}	$|\sigma_{33}-\sigma_{11}|$
Fe(P)(CO)(1-MeIm)	X-ray	−2.49	−156.9	−155.0	304.5	461.4	−4.40	−224.7	−224.4	435.9	660.6
	X-ray riding	−12.8	−172.0	−170.1	303.6	475.6	−27.3	−258.4	−257.6	434.1	692.5
	opt[b]	−30.0	−197.6	−196.1	303.7	501.3	−71.6	−323.6	−322.8	431.6	755.2
	opt BPW91	−33.6	−203.1	−200.9	303.2	506.3	−74.6	−328.8	−326.8	431.7	760.5
	opt BPW91[c]	−34.7	−204.9	−203.5	304.4	509.3	−73.3	−327.2	−325.2	432.4	759.6
	opt B3LYP	−29.2	−196.6	−194.9	303.7	500.3	−68.9	−320.0	−318.7	432.0	752.0
Fe(P)(CO)(py)	X-ray	−24.0	−188.4	−185.1	301.5	489.9	−54.6	−296.6	−294.0	426.7	723.3
	opt BPW91	−34.6	−204.1	−201.0	301.3	505.4	−79.5	−333.7	−330.0	425.2	758.9
	opt B3LYP	−30.3	−197.9	−194.5	301.5	499.4	−73.8	−324.7	−322.0	425.2	749.9
Ru(P)(CO)(1-MeIm)	X-ray	1.7	−179.1	−176.1	360.4	539.5	23.9	−239.3	−235.3	546.5	785.8
	X-ray riding	−8.10	−193.7	−190.6	360.1	553.8	−1.53	−277.9	−273.3	546.6	824.5
	opt BPW91	−6.3	−191.0	−188.0	360.2	551.2	−2.2	−277.8	−273.4	544.7	822.5
	opt B3LYP	−3.0	−186.0	−183.1	360.2	546.2	3.8	−268.2	−263.9	543.4	811.6
Ru(P)(CO)(py)	X-ray	0.1	−178.5	−177.6	356.4	534.9	16.3	−243.8	−242.3	534.9	778.7
	opt BPW91	−7.7	−190.0	−189.1	356.1	546.1	−8.4	−280.0	−278.4	533.2	813.2
	opt B3LYP	−4.3	−184.9	−183.9	355.9	540.8	−2.2	−270.0	−268.5	531.8	801.8
Os(P)(CO)(1-MeIm)	X-ray	36.4	−160.2	−157.3	426.8	587.0	115.9	−195.5	−189.6	732.9	928.4
	X-ray riding	29.5	−171.8	−168.8	429.1	600.9	99.8	−224.9	−218.6	742.7	967.6
	opt BPW91	30.6	−169.5	−166.7	428.0	597.5	95.6	−225.8	−219.5	732.0	957.8
	opt B3LYP	33.3	−165.3	−162.5	427.6	592.9	100.6	−216.4	−210.3	728.6	945.0
Os(P)(CO)(py)	X-ray	21.0	−172.2	−171.6	407.0	579.2	81.6	−225.2	−220.4	690.3	915.5
	X-ray riding	13.2	−183.9	−183.2	406.6	590.5	61.4	−257.4	−252.2	694.0	951.4
	opt BPW91	23.0	−169.5	−169.1	407.6	577.1	72.7	−232.3	−228.3	678.6	910.9
	opt B3LYP	25.7	−165.2	−164.9	407.4	572.6	78.3	−222.6	−218.7	676.1	898.7

[a] The basis set schemes used were LANL2DZ ECP on the metal, 6-311++G(2d) on the CO ligand, 6-31G* on the five nitrogen atoms bound to the metal, and 3-21G* on the remaining atoms. [b] Structure optimized at the DFT/B3LYP level with the Fe Wachters basis set (see text). [c] The basis sets used were LANL2DZ ECP on Fe, 6-311++G(2d) on the CO ligand, and 6-31G* on the remaining atoms (this calculation shows the effect of using a locally dense scheme on the chemical shielding).

We next carried out a ^{13}C and ^{17}O nuclear magnetic resonance spectroscopic investigation of both ^{13}CO- and C^{17}O-labeled metalloporphyrins, using "magic-angle" sample spinning (MAS), to deduce the principal components of the ^{13}C shielding tensor, the solid-state ^{17}O chemical shift, and the absolute magnitude of the ^{17}O nuclear quadrupole coupling constant, e^2qQ/h. In addition, we used density functional theory (DFT) to predict these same parameters, which provides an important test of our ability to predict spectroscopic observables in relatively well characterized materials.

In Figure 4 we show representative ^{13}C and ^{17}O MAS NMR spectra, in this case of Ru(TPP)(^{13}CO)(1-MeIm) and Ru(TPP)-(C^{17}O)(1-MeIm). Numerous additional ^{13}C NMR spectra at different spinning speeds were obtained on each of the six systems of interest, and the principal components of the chemical shift tensor, δ_{ii}, were derived by using the Bayesian probability/ Herzfeld−Berger method[54] described elsewhere.[49] A compilation of the experimental results is given in Table 3. We also determined the isotropic chemical shifts for ^{17}O, together with estimates of the ^{17}O nuclear quadrupole coupling (e^2qQ/h), using in this case a nutation method.[55] For ^{17}O, the relatively long T_1 values and only moderate spectral signal-to-noise ratios made combined CSA−e^2qQ/h determinations using other methods, such as satellite transition spectroscopy,[56] less practical, and since signal-to-noise ratios in proteins−the main long-term targets of our research−are far worse, this approach was not pursued.

The first observation to be made from the results shown in Table 3 is that there are very pronounced increases in both ^{13}C

and ^{17}O shieldings as one goes from Fe to Ru to Os. These increases correlate in a remarkably linear fashion with the infrared vibrational stretch frequency, ν_{CO}, as shown in Figure 5, especially for ^{17}O, where an R^2 value for the IR−NMR correlation of 0.992 is obtained. These correlations are very different from those seen in Fe−CO-containing metalloproteins, where the chemical shift changes seen over the same 100 cm^{-1} ν_{CO} range are much smaller, Figure 5, and for ^{13}C have the opposite sign. In these systems, electrostatic polarization and not "back-bonding" seems to be a more reasonable description of the spectroscopic changes seen experimentally, and indeed the inclusion of weak electrical perturbations in DFT calculations has recently permitted the relatively accurate description of the experimental shielding/ν_{CO} relationships seen in proteins.[57]

The second point of note in Table 3 is that the ^{13}C shielding tensors have remarkably similar breadths, about 470 ppm, independent of metal or axial base, and all are axially symmetric or close to axially symmetric, given a ~15 ppm experimental uncertainty in each tensor element determination. As we show below and elsewhere,[58] the small asymmetries observed in the Fe compounds arise, we believe, primarily from experimental errors, since we have been unable to reproduce them in any calculations, even though the ^{13}C tensor breadths or spans and the ^{13}C and ^{17}O isotropic shifts as well as the ^{17}O e^2qQ/h values are well reproduced.

We therefore next investigated to what extent the experimental shifts and shift (or shielding) tensor elements for the Fe, Ru, and Os systems can be predicted theoretically by using density functional theory, as embodied in the Gaussian 94 program, using the six experimental metalloporphyrin structures. To do so, we first examined the calculated ^{13}C and ^{17}O shifts of the CO ligand in the Fe(TPP)(CO)(1-MeIm) system. We

(54) Herzfeld, J.; Berger, A. *J. Chem. Phys.* **1980**, *73*, 6021−6030.

(55) Freude, D.; Haase J. In *NMR Basic Principles and Progress*; Fluck, E., Günther, H., Kosfeld, R., Seelig, J., Eds.; Springer-Verlag: Berlin, 1993; Vol. 29, pp 3−90.

(56) Jäger, C. In *NMR Basic Principles and Progress*; Fluck, E., Günther, H., Kosfeld, R., Seelig, J. Eds.; Springer-Verlag: Berlin, 1994; Vol. 31, pp 133−170.
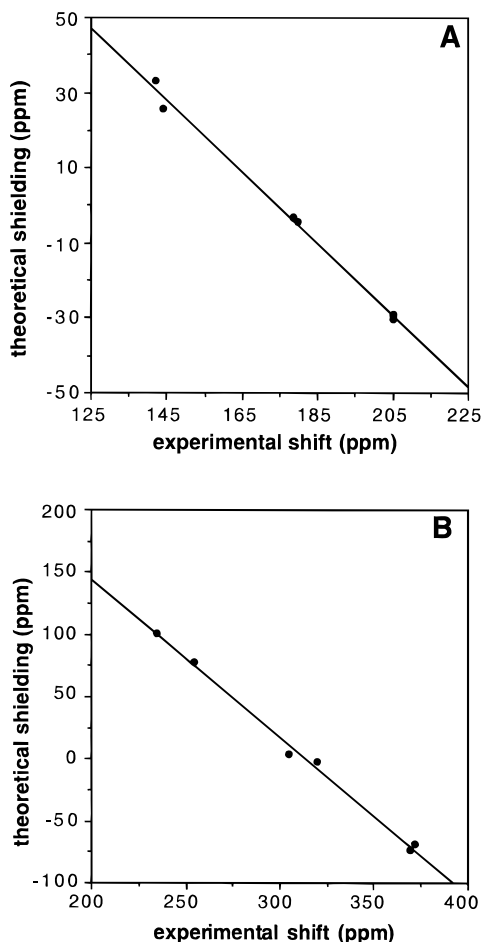
(57) deDios, A.; Earle, E. *J. Phys. Chem.* **1997**, *101*, 8132−8134.

(58) McMahon, M.; deDios, A.; Godbout, N.; Salzmann, R.; Laws, D. D.; Le, H.; Havlin, R. H.; Oldfield, E. *J. Am. Chem. Soc.* **1998**, *120*, 4784−4797.

Figure 6. Graphs showing correlations between experimental chemical shifts and theoretical shieldings for carbon-13 and oxygen-17 nuclei in carbonyl metalloporphyrin model systems. (A) Carbon-13 NMR correlations. The R^2 value is 0.994, and the slope is −0.956. (B) Oxygen-17 NMR correlations. The R^2 value is 0.995, and the slope is −1.27. Calculations were carried out using the BPW91 functional in Gaussian 94, as described in the text, using the B3LYP locally dense/ECP structures having the Fe−C and C−O bond lengths given in Table 5.

Table 7. Summary of Theory-versus-Experiment Slope and R^2 Values for ^{13}C and ^{17}O Isotropic Shifts and ^{17}O Nuclear Quadrupole Coupling Constant (NQCC) Results for X-ray and DFT Geometry-Optimized Structures[a]

structures		slope	R^2
X-ray	δ_i ^{13}C	−0.6870	0.840
	δ_i ^{17}O	−1.0220	0.910
	NQCC ^{17}O	2.0180	0.653
X-ray riding	δ_i ^{13}C	−0.5972	0.841
	δ_i ^{17}O	−0.9022	0.908
	NQCC ^{17}O	1.4933	0.623
BPW91	δ_i ^{13}C	−0.9822	0.994
	δ_i ^{17}O	−1.2727	0.995
	NQCC ^{17}O	0.6083	0.980
B3LYP	δ_i ^{13}C	−0.9562	0.994
	δ_i ^{17}O	−1.2689	0.995
	NQCC ^{17}O	0.8590	0.949

[a] Properties evaluted with the BPW91 exchange-correlation functional, as discussed in the text.
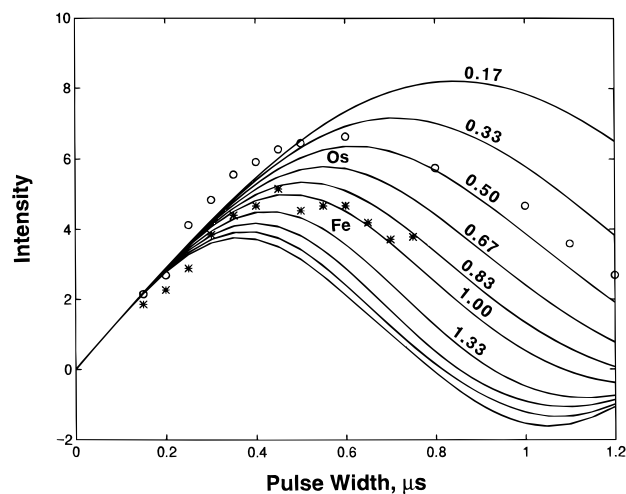

Figure 7. Experimental and theoretical ^{17}O NMR nutation plots. The open circles represent data points for carbonyl(1-methylimidazole)-(5,10,15,20-tetraphenylporphyrinato)osmium(II) while the asterisks represent nutation data for carbonyl(1-methylimidazole)(5,10,15,20-tetraphenylporphyrinato)iron(II). The solid lines represent theoretical nutation plots, and representative quadrupole coupling constants (in MHz) are indicated. In the nutation calculations, an asymmetry parameter of 0 was used.

investigated the effects on shielding of (i) the structure of the model porphyrin, (ii) the use of all-electron basis sets versus effective core potentials for the metal, and (iii) the use of various locally dense basis set schemes. The use of ECPs in ligand shift calculations is supported by the work of Kutzelnigg,[59] who has shown that contributions from core electrons on one center to the shielding tensors on neighboring nuclei are negligible. There are also several reports in the literature of ligand ^{13}C and ^{17}O chemical shifts in transition-metal carbonyls[60,61] and oxo-anions[62] using quasirelativistic ECPs and density functional theory. For ^{13}C, good overall agreement with experiment was found using sum-over-states density functional perturbation theory with individual gauges for localized orbitals, even for third-row transition-metal complexes, and in previous work[49] we have found for metal−olefin complexes that combined use of LANL2DZ metal ECPs and the BPW91 functional[39,40]

permits good predictions of olefin ligand shieldings, even with second and third row metals.

We therefore first consider the effects of structure, basis set, and the choice of ECP on shielding in Fe−porphyrin systems and then explore to what extent ligand shieldings can be predicted for the heavier elements, using ECPs. Results are presented in Table 4. For the metalloporphyrins listed, we find that replacement of phenyl groups by hydrogen atoms leads to no significant change in the calculated shifts (calculations 1 and 3 in Table 4), permitting a significant savings in computing time. The increasing C−O bond lengths from X-ray to riding model to DFT geometry-optimized structures are reflected in a maximum change in isotropic shift of 28.3 and 69.0 ppm for ^{13}C and ^{17}O, respectively, Table 4. We also find that using a locally dense basis set scheme on the porphyrin ring (calculations 3 and 6) is a reasonable approximation and again represents a useful time-savings. The replacement of the Wachters iron basis set with the Stuttgart ECP or the LANL2 ECP (with the modified, decontracted basis set) decreases the shifts by about 30 ppm (calculations 7 and 8). Calculation 9 indicates that the LANL2 is best used with the DZ basis set without modification. With the LANL2DZ ECP/basis set, calculations 10 and 11 show

(59) Kutzelnigg, W.; Fleischer, U.; Schindler, M. in *NMR Basic Principles and Progress*; Springer-Verlag: Berlin, 1990; Vol. 29, pp 165−262.
(60) Kaupp, M.; Malkin, V. G.; Malkina, O. L.; Salahub, D. R. *Chem. Phys. Lett.* **1995**, *235*, 382−388.
(61) Kaupp, M.; Malkin, V. G.; Malkina, O. L.; Salahub, D. R. *Chem.−Eur. J.* **1996**, *2*, 24−30.
(62) Kaupp, M.; Malkin, V. G.; Malkina, O. L.; Salahub, D. R. *J. Am. Chem. Soc.* **1995**, *117*, 1851−1852.

Table 8. G94/DFT BPW91[a] Oxygen-17 Electric Field Gradient Tensor Elements and Theoretical and Experimental Quadrupolar Coupling Constants for CO and Model Porphyrins

system		V_{11} (au)	V_{22} (au)	V_{33} (au)	e^2qQ/h (MHz) calc	e^2qQ/h (MHz) expt
free CO		−0.3534	−0.3534	0.7068	4.25	(+)4.40
Fe(TPP)(CO)(1-MeIm)	X-ray	−0.2743	−0.2655	0.5398	3.24	
	X-ray riding	−0.1275	−0.1178	0.2452	1.5	
	opt[b]	−0.0733	−0.0578	0.1311	0.78	(+)1.0
	opt BPW91	−0.0167	−0.0041	0.0208	0.12	
	opt BPW91[c]	−0.0155	−0.0007	0.0163	0.10	
	opt B3LYP	−0.0852	−0.0726	0.1578	0.91	
Ru(TPP)(CO)(1-MeIm)	X-ray	−0.0439	−0.0373	0.0812	0.49	
	X-ray riding	−0.1062	0.0492	0.0569	−0.64	
	opt BPW91	−0.0335	0.0130	0.0205	−0.20	(+)0.68
	opt B3LYP	−0.0378	−0.0227	0.0606	0.35	
Os(TPP)(CO)(1-MeIm)	X-ray	−0.0386	0.0065	0.0321	−0.23	
	X-ray riding	−0.1905	0.0862	0.1043	−1.1	
	opt BPW91	−0.1274	0.0542	0.0730	−0.77	(−)0.40
	opt B3LYP	−0.0661	0.0227	0.0434	−0.38	
Fe(TPP)(CO)(py)	X-ray	−0.1182	−0.1100	0.2282	1.37	
	opt BPW91	−0.0184	−0.0097	0.0281	0.17	NM
	opt B3LYP	−0.0845	−0.0763	0.1608	0.97	
Ru(TPP)(CO)(py)	X-ray	−0.0528	−0.0379	0.0907	0.54	
	opt BPW91	−0.0242	0.0050	0.0192	−0.14	NM
	opt B3LYP	−0.0378	−0.0227	0.0606	0.36	
Os(TPP)(CO)(py)	X-ray	−0.2198	0.0939	0.1259	−1.32	
	X-ray riding	−0.3868	0.1768	0.2100	−2.32	
	opt BPW91	−0.1138	0.0416	0.0723	−0.68	NM
	opt B3LYP	−0.0503	0.0108	0.0400	−0.30	

[a] The basis set schemes used were LANL2DZ on the metals, 6-311++G(2d) on the CO ligand, 6-31G* on the nitrogens bound to the metal, and 3-21G* on the remaining atoms. [b] Structure optimized at the DFT/B3LYP level with the Fe Wachters basis set (see text). [c] LANL2DZ on Fe, 6-311++G(2d) on CO, and 6-31G* on the remaining atoms.

Table 9. G94/DFT BPW91[a] Calculated ^{13}C and ^{17}O Shieldings for Fe(P)(CO)(1-MeIm) as a Function of M−C and C−O Bond Lengths

r(M−C) (Å)	r(C−O) (Å)	^{13}C shielding (ppm) σ_{11}	σ_{22}	σ_{33}	δ_i	^{17}O shielding (ppm) σ_{11}	σ_{22}	σ_{33}	δ_i
1.74	1.10	−173.6	−171.3	303.6	199.8	−252.9	−251.6	435.5	331.0
1.77	1.10	−174.2	−172.1	303.7	200.2	−259.7	−258.6	434.6	335.9
1.80	1.10	−174.6	−172.8	303.6	200.6	−265.9	−265.0	433.6	340.4
1.74	1.13	−186.8	−184.6	303.3	208.7	−285.1	−283.5	433.9	352.9
1.77	1.13	−187.8	−185.7	303.6	209.3	−292.6	−291.2	433.2	358.2
1.80	1.13	−188.6	−186.7	303.6	209.9	−299.6	−298.5	432.5	363.2
1.74	1.16	−199.9	−197.7	303.2	217.5	−319.6	−317.6	432.2	376.3
1.77	1.16	−201.2	−199.2	303.5	218.3	−328.0	−326.3	431.7	382.2
1.80	1.16	−202.4	−200.6	303.6	219.1	−335.8	−334.4	431.2	387.6

[a] The basis set schemes used were LANL2DZ ECP on the metal, 6-311++G(2d) on the CO ligand, 6-31G* on the five nitrogen atoms bound to the metal, and 3-21G* on the remaining atoms.

that the size of the calculation can again be reduced by using 6-31G* basis sets on the metal-coordinated nitrogen atoms and a locally dense scheme for the porphyrin ring. Calculations on the Fe, Ru, and Os systems were therefore carried out as in calculation 11: the metals were represented by the LANL2DZ ECP/basis sets (as found in Gaussian 94), 6-311++G(2d) basis sets were used for the CO ligand, 6-31G* for the metal-coordinated nitrogen atoms, and 3-21G* for the remaining atoms.

As can be seen in Table 4, closest accord with experiment is obtained when an all-electron basis set and either the geometry-optimized Fe(TPP)(CO)(1-MeIm) (calculation 2) or C_2Cap structure (calculation 5) are used. The riding model is close to these results, but the ^{17}O shift is almost 40 ppm in error (calculation 1) and the X-ray geometry is even more in error (calculation 4). Also notable is the close similarity in ^{13}C and ^{17}O shieldings between the all-electron calculation (1) and the much smaller ECP calculation (11).

The fact that the all-electron and LANL2 ECP calculations both show good agreement with experiment, using a geometry-optimized structure, then led us to carry out similar restrained geometry optimizations on each of the Ru and Os complexes.

To test whether the choice of functional might also be important in the optimization, we investigated both BPW91 and B3LYP functionals, and results for the M−C and C−O bond lengths are shown in Table 5. On the basis of previous geometry optimizations of tilted and bent Fe−C−O systems both by ourselves[63] and others,[24,25] a linear geometry was retained, since the global energy minimum occurs at this geometry.[24,25,63] As can be seen in Table 5, there is generally good agreement between the B3LYP and BPW91 optimizations and the X-ray values. The only exception is in the case of the Fe(P)(CO)-(MeIm) optimization, which at both B3LYP and BPW91 has a significantly longer C−O bond than the X-ray or riding geometry refinement. As for the M−C bond, the optimized BPW91 and B3LYP bond lengths are in agreement and are longer than the corresponding X-ray values, except for those of the Fe compounds with the BPW91 functional. The use of a locally dense basis set scheme and that of an effective core potential versus an all-electron basis set for the metal were found to cause no significant differences in the optimized structures. Moreover, as may be seen in Table 5 (footnotes *b* and *c*), the

(63) Havlin, R. H.; Godbout, N.; Salzmann, R.; Wojdelski, M.; Arnold, W.; Schulz, C. E.; Oldfield, E. *J. Am. Chem. Soc.* **1998**, *120*, 3144−3151.
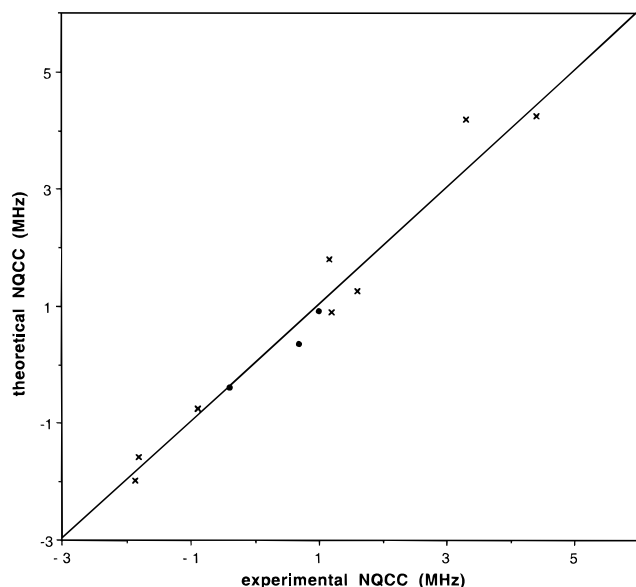
Figure 8. Graph showing correlation between experimental oxygen-17 nuclear quadrupole coupling constants and those computed theoretically. The crosses indicate data for simple metal carbonyls and metal clusters.[64] The solid circles represent data for the three carbonyl 1-methylimidazole metalloporphyrins. The signs of the experimental nuclear quadrupole coupling constants were taken from the theoretical calculations. The solid line shows the ideal 1:1 experiment-versus-theory correlation line.

differences between using locally dense and more uniform basis sets (footnote *b*, BPW91 calculation) and between the use of the Wachters all-electron basis and the use of the LANL2DZ ECP basis are essentially zero. In what follows, we therefore use the locally dense/ECP optimized structures, for property predictions.

We show in Table 6 the results of DFT shielding tensor calculations for both crystallographic and DFT geometry-optimized structures, the latter having the M−C and C−O bond lengths shown in Table 5. There is very good overall agreement between the computed and experimental results when DFT optimized structures are used, and a typical set of ^{13}C and ^{17}O isotropic shift results are shown in Figure 6. The slope of the shift/shielding correlation using the B3LYP optimized structure is −0.956 for ^{13}C with an R^2 value of 0.994, to be compared with the ideal values of −1 and 1, respectively. For ^{17}O, we find a slope of −1.269 and an R^2 value of 0.995, a slightly worse slope than with ^{13}C, but nevertheless the R^2 value is extremely high. Basically similar results are obtained when the BPW91 geometry-optimized structures are used, as shown in Table 7, although, as expected, results determined for the X-ray structure are slightly worse, with a ^{13}C slope of −0.69 and an R^2 value of 0.84, as shown in Table 7. For the iron-containing systems, there is relatively good agreement between calculated and experimental values of the shift anisotropies or tensor spans. The average computed $|\sigma_{33} - \sigma_{11}|$ for the two bases is comparable to an experimental value of ∼468 ppm. It is interesting that in none of our shielding calculations is there any appreciable asymmetry in the ^{13}C shielding tensor, even though a wide variety of metalloporphyrin/base orientations were investigated, indicating that "proximal side" effects do not change the symmetry of the tensor. Both carbon and oxygen shieldings evaluated using the LANL2DZ iron basis, with or without porphyrin phenyl groups, give results that are too shielded when the shorter C−O bond lengths are used, Tables 4 and 5.

For Ru and Os, while the isotropic shieldings computed are

in good accord with experiment, there is a fairly uniform overestimation of the span of the ^{13}C shielding tensor over that seen experimentally, Tables 3 and 6. In the future, it seems likely that the overall accord between theory and experiment may be improved somewhat from the current results, for example by using all-electron metal representations for the heavier elements. However, the current R^2 values for the isotropic shift/shielding correlation are already excellent and support the idea that DFT geometry optimization more accurately represents the real Fe−C and C−O bond lengths for Fe(TPP)(CO)(1-MeIm), since only the shieldings of the optimized structure are close to the correlation line (Figure 6). And, as we show below, the same improvement is also observed for the ^{17}O e^2qQ/h as well.

Finally, we have investigated the ^{17}O nuclear quadrupole coupling constants in the three 1-methylimidazole complexes. Because of limited signal-to-noise ratios, we used a pulse nutation technique on the central transition. Nutation plots and simulations are shown in Figure 7, and the e^2qQ/h results obtained from the simulations are presented in Table 8, together with the results of Gaussian 94 electric field gradient tensor and e^2qQ/h calculations at a variety of geometries.

In previous work,[64] we found that the ^{17}O nuclear quadrupole coupling constants in four metal carbonyls, $Fe(CO)_5$, $Fe_2(CO)_9$, $Ni_2(\eta^5\text{-}C_5H_5)_2(CO)_2$, and $Rh_6(CO)_{16}$, could be measured experimentally and predicted theoretically (using the deMon/DFT approach) with an rms error of 0.37 MHz (for a total of seven points), a theory-versus-experiment slope of 1.09, and an R^2 value of 0.959,[64] which gives some idea as to the combined accuracy of e^2qQ/h nutation measurements and DFT calculations. These points are shown in Figure 8 (+) together with the Gaussian 94 Fe, Ru, and Os $C^{17}O$−TPP complex e^2qQ/h results (●), obtained using the B3LYP geometry-optimized structure. Here, we must note that the signs of all experimental e^2qQ/h results are taken from the calculations, as we have done previously with the simpler model systems,[64] since the signs cannot be determined from the nutation experiment. As can be seen from Table 8 and Figure 8, there is good agreement between the experimental and theoretical results when the B3LYP DFT geometry-optimized structure is used, with an rms error between theory and experiment of only 0.20 MHz, well within the 0.37 MHz rmsd found previously (which derived from a much larger range of nuclear quadrupole coupling constants and a broader variety of compounds). For calculations performed at the X-ray geometries (Table 5), there is also good accord with experiment, but there are noticeable deviations for the BPW91 optimized structures, Table 8, an effect which can be attributed to the uniformly longer C−O bond lengths in the BPW91 structures, Table 5. We show each of these correlations in Table 7, together with the ^{13}C and ^{17}O shielding results, from which it can be seen that we obtain the best, overall, description of the ^{13}C and ^{17}O shifts and the ^{17}O electric field gradient tensor by use of B3LYP geometry-optimized structures, which are also those which are closest to the conventional X-ray structures (except in the case of Fe(TPP)(CO)(1-MeIm)). However, it is not immediately obvious from the results obtained so far just which bond lengths, metal−carbon ($r(M-C)$) or carbon−oxygen ($r(C-O)$), dominate the shielding and electric field gradient results observed. We therefore computed the ^{13}C and ^{17}O shieldings and ^{17}O electric field gradients as a function of $r(M-C)$ and $r(C-O)$ for the nine selected geometries given in Tables 9 and 10. These parameter calculations were then converted into the three corresponding property surfaces for the Fe(P)(CO)(1-MeIm) complex: δ^O ($r(M-C),r(C-O)$), δ^C ($r(M-$

(64) Salzmann, R.; Kaupp, M.; McMahon, M.; Oldfield, E. *J. Am. Chem. Soc.* **1998**, *120*, 4771−4783.

Table 10. G94/DFT BPW91[a]Calculated ^{17}O Electric Field Gradient and Nuclear Quadrupole Coupling Constants in Fe(P)(CO)(1-MeIm) as a Function of M−C and C−O Bond Lengths

r(M−C) (Å)	r(C−O) (Å)	electric field gradient			
		V_{11} (au)	V_{22} (au)	V_{33} (au)	NQCC (MHz)
1.74	1.10	−0.1714	−0.1601	0.3316	1.99
1.77	1.10	−0.1824	−0.1710	0.3534	2.12
1.80	1.10	−0.1931	−0.1816	0.3746	2.25
1.74	1.13	−0.1022	−0.0900	0.1922	1.16
1.77	1.13	−0.1135	−0.1012	0.2148	1.29
1.80	1.13	−0.1246	−0.1122	0.2368	1.42
1.74	1.16	−0.0320	−0.0191	0.0511	0.31
1.77	1.16	−0.0441	−0.0310	0.0751	0.45
1.80	1.16	−0.0559	−0.0425	0.0984	0.59

[a] The basis set schemes used were LANL2DZ ECP on the metal, 6-311++G(2d) on the CO ligand, 6-31G* on the five nitrogen atoms bound to the metal, and 3-21G* on the remaining atoms.
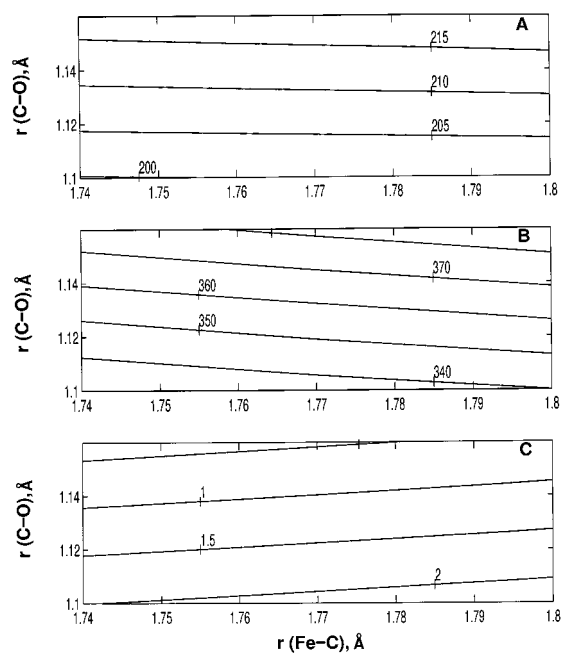
Figure 9. Property surfaces as a function of M−C and C−O bond lengths: (A) ^{13}C shift surface; (B) ^{17}O shift surface; (C) ^{17}O nuclear quadrupole coupling constant surface. The calculations are for Fe(P)-(CO)(1-MeIm) so M = Fe; the axes are in Å.

C),r(C−O)) and NQCC (r(M−C),r(C−O)). These surfaces are shown in Figure 9. As may be seen from the figure, all properties are overwhelmingly dominated by changes in r(C−O), the ligand bond length. Thus, any inaccuracies in the crystallographic determinations of C−O bond lengths are predicted to have a major influence on the computed ligand properties, but the effect is much smaller for changes in M−C bonding. More quantitatively, we can deduce metric shielding derivatives, $\partial\sigma/\partial r$, for both ^{13}C and ^{17}O in the Fe(TPP) species. We find $\partial\sigma_C/\partial r_{C=O} \sim -300$ ppm/Å and $\partial\sigma_O/\partial r_{C=O} \sim -800$ ppm/Å, values which are to be compared with $\partial\sigma_C/\partial r_{C=O} = -418$ ppm/Å and $\partial\sigma_O/\partial r_{C=O} = -900$ ppm/Å for free CO gas (data not shown), while the Fe−C shielding derivatives are much smaller, about −20 ppm/Å for ^{13}C and about −190 ppm/Å for ^{17}O, at the optimized geometry.

Conclusions

First, we have described the synthesis and structural characterization of three new metalloporphyrins in the Fe, Ru, Os series, which permits a structural comparison of all of the six CO complexes which can be prepared from TPP, 1-MeIm, and pyridine. The results indicate large saddle distortions in all three

1-methylimidazole complexes—about an order of a magnitude larger than those for the three corresponding pyridine systems. Second, we have determined the solid-state ^{13}C NMR chemical shifts and shift tensors, as well as the ^{17}O NMR isotropic chemical shifts, for all six systems. We find remarkably good empirical correlations between the isotropic chemical shifts and the vibrational stretch frequency, ν_{CO}, trends which are quite different from those seen previously in metalloproteins, which appear to be dominated by electrostatic field effects.[57,58] Third, we have used density functional theory to begin to investigate the experimental shifts. We find a very good correlation between theory and experiment, with R^2 values of >0.99 being found for both ^{13}C and ^{17}O NMR. Fourth, we have used a nutation method to determine the overall magnitude of the nuclear quadrupole coupling constant. There is very good agreement (rmsd = 0.20 MHz) between these results and those of the DFT calculations, when DFT geometry-optimized structures are employed.

The ability to predict the ^{13}C and ^{17}O NMR spectroscopic observables in metalloporphyrins is an important first step in using NMR and quantum chemistry to predict, refine, and determine molecular structures in metalloproteins, where knowledge of structural−spectroscopic correlations can help answer long-standing questions about metal−ligand interactions.[58,63,65]

Supporting Information Available: Tables of crystal data, structure solution and refinement details, atomic coordinates, anisotropic displacement parameters, hydrogen coordinates, bond lengths and angles, and torsion angles (60 pages, print/PDF). X-ray crystallographic files, in CIF format, are available on the Internet only. See any current masthead page for ordering information and Web access instructions.

(65) Godbout, N.; Havlin, R.; Salzmann, R.; Debrunner, P. G.; Oldfield, E. *J. Phys. Chem. A* **1998**, *102*, 2342−2350.